CHEMISTRY OF MATERIALS

Article

pubs.acs.org/cm

Thiophene Polymer-Grafted Barium Titanate Nanoparticles toward Nanodielectric Composites

Yali Qiao,[†] Md. Sayful Islam,[‡] Lei Wang,[†] Yi Yan,[†] Jiuyang Zhang,[†] Brian C. Benicewicz,[†] Harry J. Ploehn,[‡] and Chuanbing Tang*[,†]

[†]Department of Chemistry and Biochemistry and [‡]Department of Chemical Engineering, University of South Carolina, Columbia, South Carolina 29208, United States

Supporting Information

ABSTRACT: This paper reports a strategy for controlling surface chemistry of barium titanate ($BaTiO_3$) using surface-initiated reversible addition−fragmentation chain transfer (RAFT) polymerization of an oligothiophene monomer. The modular chemistry on the engineering of nanoparticles provides a facile pathway to compatibilizing dielectric nanofillers in a matrix of oligothiophene polymers, leading to the formation of nanodielectric composites with permittivity at ∼20 and dielectric loss <0.02 over a wide range of frequencies (1 kHz to 1 MHz). This approach could be generalized to a variety of nanoparticles with tunable dipolar polymer shells for the development of novel dielectric nanocomposite systems for energy storage.

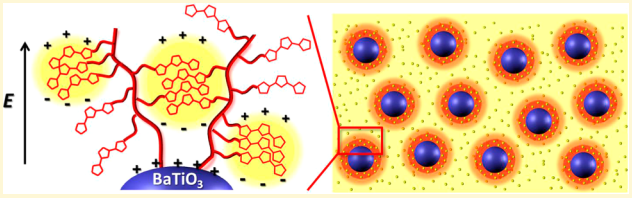

I. INTRODUCTION

Novel dielectric materials for energy storage are of great interest due to their potential applications in portable electronic devices, hybrid electric vehicles, power electronics for grid energy management, and pulsed power systems.[1−4] Traditionally, inorganic ceramics have been extensively used due to their super high dielectric permittivity.[5−8] However, they possess low breakdown strength and high dielectric loss, which make them impractical for long lifetime energy storage. Considering these limitations, polymers[9−18] have been broadly explored as alternative dielectric materials.[19−24] Polymers exhibit high breakdown strength, low dielectric loss, better mechanical properties, facile processability, and lighter weight. However, most polymers have relatively low permittivities (e.g., 2−5) compared to dielectric inorganic ceramics.

Recently, polymer composite dielectrics have gained much attention because they offer a compromise of the best properties of ceramic and polymer dielectrics.[25−27] Approaches include the addition of high permittivity inorganic fillers (e.g., $BaTiO_3$)[28−31] or conductive/semiconductive fillers (e.g., conductive polymers, carbon nanotubes)[32−38] to polymers with high breakdown strength. Among them, introduction of inorganic nanoparticles into polymer matrices to form dielectric polymer nanocomposites represents one of the most promising and exciting approaches to achieving high-performance dielectrics. Composites based on ferroelectric poly(vinylidene fluoride) (PVDF) and its copolymers have been studied widely because both the polymer and inorganic fillers may contribute significantly to the permittivity.[38−45] While most of the current studies on dielectric nanocomposites are focused on the enhancement of dielectric permittivity, these systems often suffer from high dielectric loss, limiting their practical use for energy storage.[19−21]

Polymer nanocomposites[3,46−48] can be fabricated via solution mixing or mechanical blending, in situ polymerization, and in situ nanoparticle synthesis.[25−27] For most strategies, the incompatibility between inorganic nanoparticles and polymers is a challenging problem and usually leads to nanoparticle agglomeration, macrophase separation, voids, etc., which has a negative effect on the dielectric properties. Consequently, the resulting inhomogeneous films often display high dielectric loss and low breakdown strength. Covalent grafting of polymer chains from inorganic nanoparticle surfaces has proven to be a promising approach, leading to improved dispersion in a polymer matrix and thus enhanced dielectric properties.[43,46,49,50]

Herein we report the synthesis of novel barium titanate ($BaTiO_3$ or BT) based hybrid nanoparticles, which were surface-modified precisely with dithioesters via a key activation-installation step. Robust surface-initiated reversible addition−fragmentation chain transfer (RAFT) polymerization was carried out using a conjugated heteroaromatic oligomer-containing monomer with an elegant control on polymerization kinetics. We chose 2-(2,2′:5′,2″-terthien-5-yl)ethyl methacrylate (TTEMA) as the monomer. Our recent work showed that TTEMA polymers (PTTEMA) have comparable permittivity to PVDF (e.g., > 10),[51] while they can self-organize into polarizable crystalline domains at a scale of only 1−2 nm that are critical for dielectric loss control.

Received: June 28, 2014
Revised: August 27, 2014
Published: August 28, 2014

 © 2014 American Chemical Society dx.doi.org/10.1021/cm502341n | Chem. Mater. 2014, 26, 5319−5326

II. RESULTS AND DISCUSSION

Synthesis of Surface-Modified $BaTiO_3$ Nanoparticles by RAFT. The synthetic route for the surface modification of the as-received BT nanoparticles is shown in Scheme 1a. The enrichment of hydroxyl groups on the surface of the nanoparticles was achieved by refluxing the as-received BT nanoparticles in hydrogen peroxide solution. Amino-group functionalized BT nanoparticles (BT-NH_2) were then prepared by refluxing hydroxyl-rich BT nanoparticles (BT-OH) with 3-aminopropyl triethoxysilane (γ-APS) in toluene.[31,41,52] Following the synthetic procedures previously reported for the preparation of 4-cyanopentanoic acid dithiobenzoate (CPDB) modified silica nanoparticles,[53,54] the carboxyl group of CPDB was first activated with 2-mercaptothiazoline, and then the activated-CPDB (see ^{1}H NMR in Figure S1) was used to selectively react with the amino group on BT nanoparticles in the presence of the thiocarbonylthio bond. Through this critical activation-installation step, CPDB was successfully attached onto BT nanoparticles, which were well characterized by FT-IR spectra (see details in Figure S2).

After the synthesis of CPDB@BT, oligothiophene-containing polymers were grafted onto the BT nanoparticles via surface-initiated-RAFT polymerization. The thickness of the polymer shell can be readily tuned by controlling the molecular weight of graft polymers. The kinetics of surface-initiated RAFT polymerization from CPDB-anchored BT nanoparticle was investigated. The terthiophene-containing monomer TTEMA was polymerized using 2,2′-azobis(isobutyronitrile) as initiator, mediated with a CPDB on BT nanoparticle surface and free CPDB system (Scheme 1b). Using a small amount of free CPDB RAFT agent enabled better control of the polymerization process to obtain low-dispersity graft polymers and limit gelation or particle aggregation.[31,41] Figure 1a shows an excellent linear relationship between $\ln([M]_0/[M])$ and time, indicating a constant radical concentration during the polymerization. The gel permeation chromatography (GPC) traces of graft polymers, which were recovered at various polymerization time after treating the polymer-grafted BT nanoparticles with aqueous HF (49%), are shown in Figure S3. Figure 1b shows that the number-average molecular weight of graft polymers increased linearly with monomer conversion, and the measured molecular weight determined by GPC was close to the theoretical value. This demonstrates the controlled/"living" graft polymerization of TTEMA. In addition, the graft polymers showed low dispersity ranging from 1.06 to 1.22 up to 40% conversion. These results demonstrated that oligothiophene-containing monomers could be efficiently polymerized from the surface of BT nanoparticles in a controlled/"living" fashion. As a result, the interface between the BT nanoparticles and the matrix can be modulated when using the same kind of shell polymers as the matrix. Following the efficient surface-initiated RAFT polymerization, two PTTEMA modified BT nanoparticles, PTTEMA1@BT with $M_{n,\ PTTEMA1}$ = 22 000 g/mol and PTTEMA2@BT with $M_{n,\ PTTEMA2}$ = 32 400 g/mol, were

Scheme 1. Synthesis of 4-Cyanopentanoic Acid Dithiobenzoate Anchored onto $BaTiO_3$ Nanoparticles and RAFT Polymerization of TTEMA on the Surface of Nanoparticles

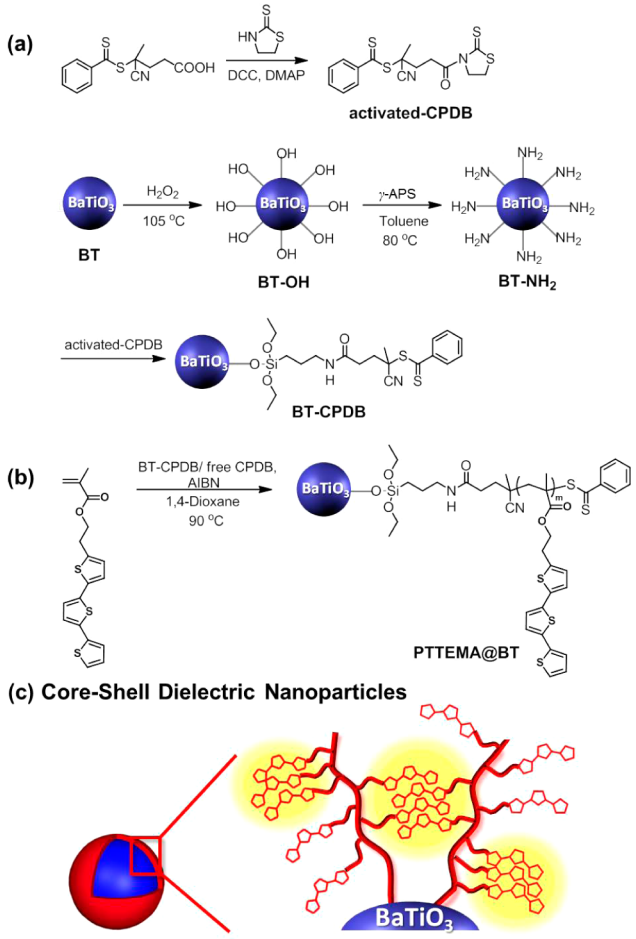

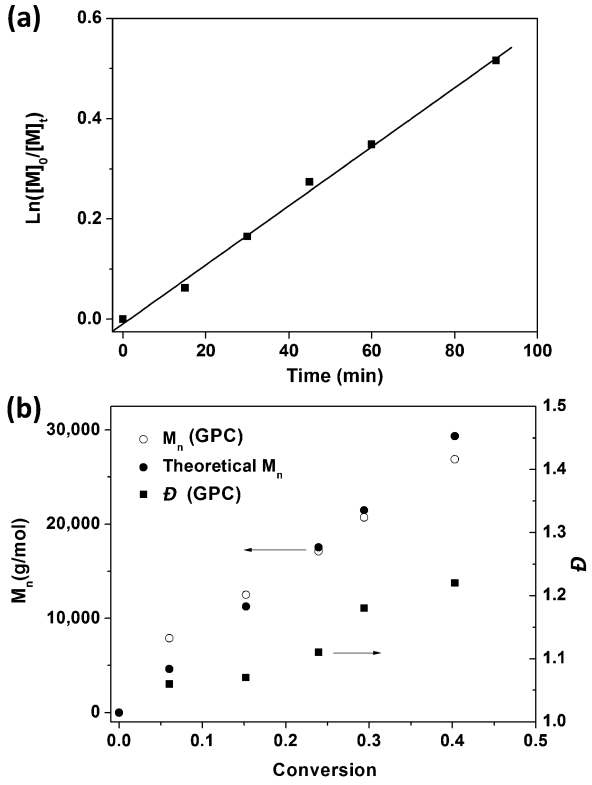

Figure 1. (a) The first-order kinetic plot; (b) Dependence of molecular weight and dispersity ($Đ$) on conversion for RAFT polymerization of terthiophene-containing TTEMA monomer mediated with CPDB-functionalized BT nanoparticles.

dx.doi.org/10.1021/cm502341n | Chem. Mater. 2014, 26, 5319−5326

prepared. Molecular weight and molecular weight distribution of graft polymers are summarized in Table S1.

Characterization of Oligothiophene Polymer-Grafted $BaTiO_3$ and Their Nanocomposites. The morphologies of PTTEMA@BT core−shell nanoparticles were characterized by TEM (Figure 2a-c). Compared with the as-received BT

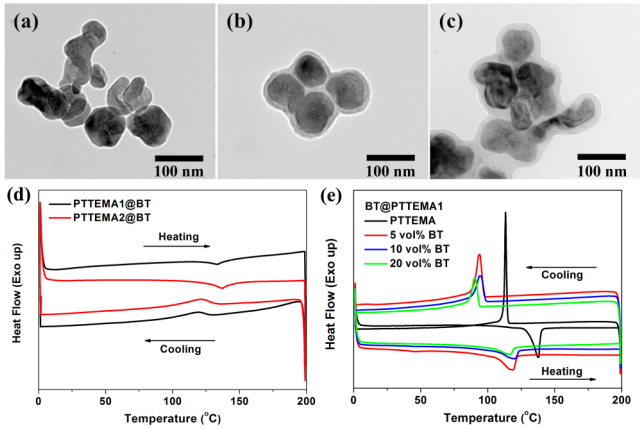

Figure 2. TEM images of (a) as-received BT nanoparticles; (b) PTTEMA1@BT; (c) PTTEMA2@BT; and DSC curves of (d) PTTEMA@BT nanoparticles; (e) BT@PTTEMA1/PTTEMA nanocomposites (upper is the exothermal direction).

nanoparticles, a stable and dense polymer shell was clearly coated on the surface of BT nanoparticles. The thickness of oligothiophene-containing polymer shells is about 8−9 nm for PTTEMA1@BT and about 14−15 nm for PTTEMA2@BT. Differential scanning calorimetry (DSC) measurements (Figure 2d) showed that the PTTEMA polymers on the particle surface could still maintain similar melting and recrystallization processes to those in free homopolymers, though the former less distinct due to the presence of a large fraction of BT nanoparticles. The crystallization temperature increased with the increase of molecular weight of the graft polymers, from 119.2 °C for PTTEMA1@BT to 121.6 °C for PTTEMA2@BT (data shown in Table S1). Additionally, the melting points showed similar tendency with the change of molecular weight. Both tendencies of the crystallization temperature and melting point with the molecular weight were quite similar to those of the homopolymers we reported earlier.[51] These results suggested that the graft polymers could still maintain their thermal properties after attachment onto the BT nanoparticles.

The oligothiophene-containing polymer based nanocomposite films with various volume fractions (5, 10, and 20 vol %) of BT nanoparticles were prepared by solution blending of the PTTEMA-grafted BT nanoparticles and a PTTEMA homopolymer matrix (M_n = 25 200 g/mol). The surface morphology of nanocomposite films was examined by atomic force microscopy (AFM). As shown in Figure 3, BT nanoparticles could be readily recognized for all three series of nanocomposite films, and no obvious difference in surface morphology could be observed in the height images. However, a slight variation could be distinguished through surface roughness analysis. The surface roughness R_q of the nanocomposite films slightly decreased from 6.44 nm for composites containing pristine BT to 6.02 and 6.23 nm for PTTEMA1@BT and PTTEMA2@BT based nanocomposites, respectively. Considering the average nanoparticle size (~50 nm), the roughness analyses demonstrate good quality of thin films with smooth and continuous

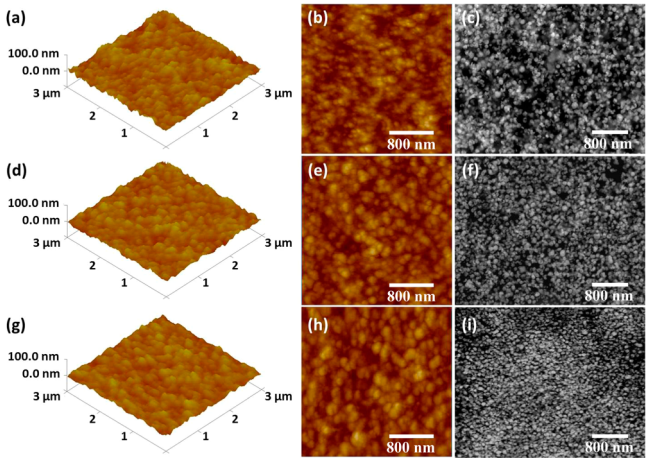

Figure 3. Representative AFM (a, b, d, e, g, h) and cross-sectional FESEM (c, f, i) images of the nanocomposite films containing (a-c) pristine BT; (d-f) PTTEMA1@BT; (g-i) PTTEMA2@BT blended with the PTTEMA homopolymer with 20 vol % loading of BT nanoparticles.

surface morphology and strongly suggest that the surface-grafted PTTEMA improves the dispersion of nanoparticles in composites. Actually, in solution state, after the attachment of PTTEMA, the nanoparticles showed much better dispersibility compared with as-received BT in many organic solvents such as toluene, THF, DMF, etc. Visual observations confirmed that the suspensions of PTTEMA1@BT and PTTEMA2@BT nanoparticles in THF were more stable after 18 h (see Figure S8).

In addition, FESEM cross-sectional images of nanocomposite films with 20 vol % of BT nanoparticles indicate the degree of microscopic homogeneity inside the nanocomposite films. As shown in Figure 3 (c, f, i), all PTTEMA-modified BT nanoparticles were well dispersed in the polymer matrix, and no obvious agglomeration could be found. In addition, more compact nanoparticle distribution and thus less obvious pores and cavities were observed in comparison with the pristine BT nanoparticle based composites. The AFM and FESEM results show that the oligothiophene-containing polymer shell might provide strong interparticle forces that improve BT nanoparticle dispersion. In addition, similar chemical structures of the graft polymer and the polymer matrix may improve the interfacial adhesion between the nanoparticles and matrix as well.

DSC and Wide-Angle X-ray Diffraction (WAXD) measurements were performed to estimate the crystalline microstructure of the PTTEMA@BT based nanocomposites in comparison with that of the matrix, aiming at understanding the effects of the inclusion of such hybrid nanoparticles on the microstructure of the PTTEMA polymer matrix. As shown in Figure 2e and Figure S7, the crystallization temperature (T_c) of all the nanocomposites shifts to lower values, and PTTEMA2@BT based nanocomposites with a thicker polymer shell showed a smaller decrease than those with a thinner polymer shell at various volume fractions of BT nanoparticles. In addition, the introduction of PTTEMA@BT nanoparticles also led to a decrease of the heat of fusion, for instance, changing from 15.25 J g^{-1} for the polymer PTTEMA matrix to 5.584 J g^{-1} and 6.284 J g^{-1} for PTTEMA1@BT and PTTEMA2@BT based nanocomposites containing 5 vol % BT nanoparticles, respectively. These results indicated a decrease of the degree of crystallinity

dx.doi.org/10.1021/cm502341n | Chem. Mater. 2014, 26, 5319−5326

resulting from the inclusion of the PTTEMA@BT nanoparticles to the PTTEMA polymer matrix. Moreover, there is a successive decrease in the heat of fusion as the volume fraction of BT nanoparticles further increased from 5 vol %, to 10 vol %, and further to 20 vol %, regardless of the polymer shell thickness for the hybrid nanoparticles, indicating a continuous decrease of degree of crystallinity with the increase of volume fraction of BT nanoparticles in the nanocomposites.

As displayed in Figure 4, although the WAXD patterns of the nanocomposites are dominated by the diffraction peaks at a 2θ

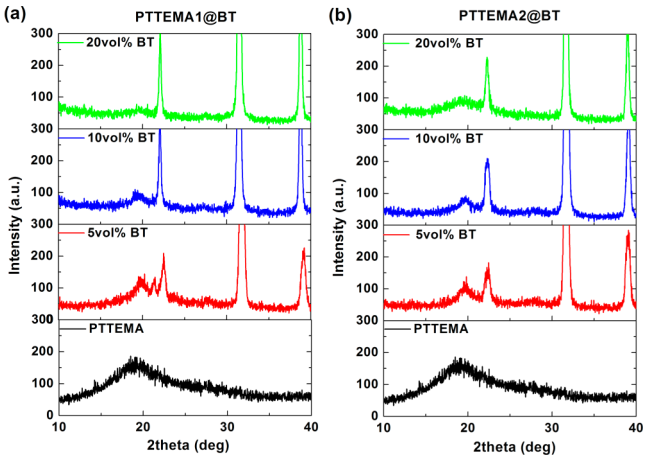

Figure 4. WXRD patterns of the surface PTTEMA-modified BT nanocomposites using (a) PTTEMA1@BT and (b) PTTEMA2@BT, including different compositions for each kind of nanocomposite compared with a pure PTTEMA homopolymer.

angle of 22.3°, 31.7°, 39.0°, and 45.3° corresponding to cubic phase $BaTiO_3$,[55] a relatively weak and broad peak at a 2θ angle of ca. 19° can still be observed, which is attributed to diffractions from the PTTEMA polymer matrix.[51] After inclusion of PTTEMA@BT nanoparticles, the main diffraction peaks become sharper with a dramatically decreased intensity. Theoretically, the crystalline domain size can be estimated from Scherrer's formula,[40,56] $t = \lambda/B \cos \theta$, where t is the crystallite size, λ is the wavelength of X-ray, B is the full width at half-maximum of diffraction peaks from JADE software, and θ is the diffraction angle. Since the diffraction peak at a 2θ angle of 22.3° from cubic phase $BaTiO_3$ was partially overlapped with that at a 2θ angle of 19° from the matrix, it is difficult to analyze the exact B values for calculation of the crystallite size of the polymer matrix in the nanocomposites. However, qualitatively, an obvious decrease of the B value for the nanocomposites could be observed when compared with that of the neat polymer matrix, while maintaining a 2θ angle at nearly the same level. Accordingly, the crystalline domain size from the polymer matrix in all the nanocomposites (estimated between 2−3 nm) showed a tendency to increase compared with that of the neat polymer matrix (~1.6 nm) with the introduction of the PTTEMA@BT nanoparticles.

The formation of crystalline domains in the terthiophene-containing polymer is believed to be induced by the interaction and self-organization between terthiophene side chains as shown in Scheme 1c,[51] and the crystalline domain sizes have a close relationship with the probability and proportionality of contact of the side-chains. With the inclusion of PTTEMA@BT nanofillers in the polymer matrix, the terthiophene side-chains in the polymer shell grafted on the surface of the nanoparticles increase the probability of accessibility of adjacent terthiophene segments either from the surface or from the polymer matrix, thus this might enhance the proportionality of the interacted side chains, both of which are beneficial for formation of larger crystalline domains. However, for both kinds of PTTEMA@BT based nanocomposites, the crystallite size from the polymer matrix slightly decreased with the increase of the volume fraction of BT nanoparticles from 5 vol % up to 20 vol %.

Dielectric Properties of Nanocomposites. Nanocomposite materials using the PTTEMA@BT hybrid nanoparticles as fillers and a PTTEMA homopolymer as matrix were fabricated and investigated as nanodielectric materials. Compared with other systems reported in the literature,[28,30,31,34,39−43,57,58] this approach has a few distinct advantages. First, the PTTEMA polymer shells have exactly the same chemical structure as the polymer matrix, which may enhance the dispersion of BT nanoparticles and improve particle−polymer interfacial adhesion. Second, the PTTEMA polymer shell can act as a buffer layer and alleviate the large contrast in permittivity between nanoparticle and polymer matrix,[31,39,41] promoting a more homogeneous electric field in the nanocomposite system, leading to high dielectric permittivity with low dielectric loss. Finally, the small nanoscale conjugated domains (<5 nm) dispersed in the PTTEMA matrix could facilitate fast polarizability response, especially at high frequency, in sharp contrast with large crystalline domains and thus slow polarizability response in PVDF.

Figure 5 shows the dielectric properties of various materials, including pristine BT, PTTEMA1@BT, and PTTEMA2@BT nanoparticles dispersed in the PTTEMA homopolymer matrix. In all cases, the relative permittivity values (ε_r) of composites (Figures 5a, 5c, and 5e) are greater than that of the pure

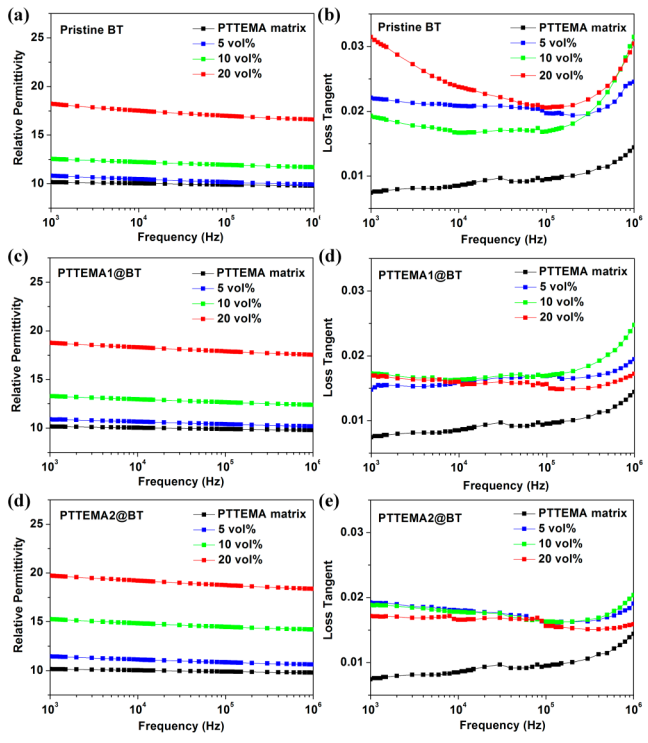

Figure 5. Dielectric property of various materials: Relative permittivity as functions of (a), (c), and (d) frequency; (b), (d), and (e) Loss tangent as functions of frequency. All measurements carried out at ambient temperature (23 °C).

dx.doi.org/10.1021/cm502341n | Chem. Mater. 2014, 26, 5319−5326

PTTEMA homopolymer and nearly independent of applied electric field frequency. The constancy of permittivity over such a wide frequency range (1 kHz to 1 MHz) is truly remarkable, compared to the significant frequency dependence of widely studied nanocomposites based on PVDF homopolymers and copolymers.[30,38−43]

As expected, ε_r values for the nanocomposites increase with BT volume fraction, reaching values twice that of the PTTEMA matrix at 20 vol % BT loading. Moreover, nanocomposites containing PTTEMA@BT hybrid nanoparticles manifested greater ε_r values than the composite containing pristine BT. Figure S9 shows that the presence of grafted PTTEMA, and its molecular weight, influences the relative permittivity. For all vol % BT loadings, ε_r values for composites containing PTTEMA@BT particles were significantly higher than those of composites containing pristine BT. Likewise, ε_r values for PTTEMA2@BT composites (higher MW graft polymer) are significantly greater than those for PTTEMA1@BT composites (lower MW graft polymer). There may be two reasons for these observations. First, the presence of the grafted PTTEMA layer probably promotes better dispersion of the BT particles, resulting in more uniform distribution of the electric field over the BT and thus higher effective permittivity. Second the grafted PTTEMA layers may influence the quantity and size of the PTTEMA crystalline domains so as to increase the density of polarizable dipoles in the polymer domain, resulting in increased permittivity.

All of the nanocomposite films exhibited dielectric loss (expressed in terms of loss tangent, tan δ, Figures 5b, 5d, and 5f) slightly higher than that of the pure PTTEMA homopolymer but still much lower compared to BT/PVDF composites.[41−43] The PTTEMA homopolymer has low tan δ values, ranging from about 0.007 to 0.014 over the 1 kHz to 1 MHz range. The tan δ values for the PTTEMA@BT nanocomposites are all less than about 0.02 over this wide frequency range. This indicates that the addition of BT to the PTTEMA polymer introduces additional dielectric loss mechanisms. However, the nearly constant tan δ and its nondependence on BT loading further intensify the robustness of our grafting strategy.

Polarization testing was carried out to investigate the dielectric properties of PTTEMA, BT/PTTEMA, and PTTEMA@BT/PTTEMA composites subjected to applied fields. Figure 6 shows typical displacement-electric field (D-E) loops. At moderate electric field strengths, the D-E loops exhibit nearly linear behavior. The slopes of the D-E loops and composite polarizability increase with the increase of nanoparticle loading (Figure 6a), as expected. Figure 6a also shows that the 20 vol % PTTEMA2@BT composite exhibits a noticeable hysteresis. Similar displacement-electric field behavior was observed for the PTTEMA1@BT composite (Figure S10).

Figure 6b compares D-E loops for 10 vol % composites prepared with BT particles having different surface treatments. The composites prepared with PTTEMA@BT have higher polarizability than those made with pristine BT. Moreover, polarizability increases with the increase of molecular weight of grafted PTTEMA (PTTEMA1@BT < PTTEMA2@BT). This is consistent with the trend seen in the relative permittivity (Figure 5a). Two explanations may be suggested. First, the presence of grafted PTTEMA may promote the formation of a greater quantity of polarizable nanocrystalline domains in the PTTEMA matrix, with higher molecular weight of the grafted

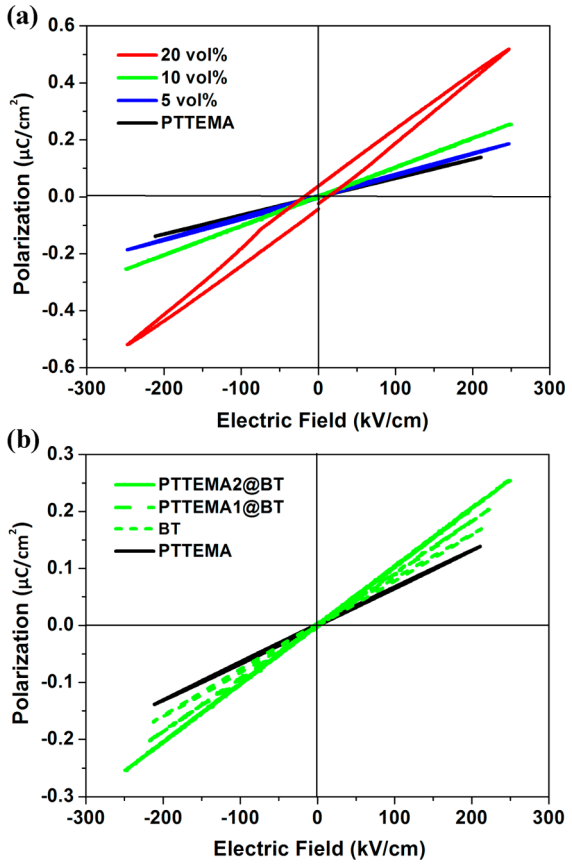

Figure 6. Polarization as a function of applied electric field for (a) a pure PTTEMA homopolymer and PTTEMA2@BT/PTTEMA nanocomposites containing varying vol % BT nanoparticles; and (b) a pure PTTEMA homopolymer and BT/PTTEMA and PTTEMA@BT/PTTEMA nanocomposites containing 10 vol % BT nanoparticles. D-E loops were measured at ambient temperature (23 °C) with 1 kHz cycle frequency.

PTTEMA more effective than the lower molecular weight. Second, the presence of grafted PTTEMA on the BT particle surface may promote better dispersion of the BT in the PTTEMA matrix, relative to pristine BT. Higher molecular weight grafted PTTEMA would provide greater steric repulsion and thus more effective BT particle dispersion than the lower molecular weight grafted polymer.

The energy density results (both stored and released energy presented in Figure S11) show that nearly all the stored energy is recovered upon cycling. Figure 7 shows the stored energy density ratio of BT/PTTEMA and PTTEMA@BT/PTTEMA nanocomposites relative to a pure PTTEMA homopolymer measured at the same electric field polarization. The energy density of all nanocomposites improved in comparison with that of the pure PTTEMA matrix at various vol % loading of BT nanoparticles. The composites prepared with PTTEMA@BT have higher energy density than those made with pristine BT. Moreover, energy density increases with the increase of molecular weight of grafted PTTEMA (PTTEMA1@BT < PTTEMA2@BT). At 20 vol % loading of BT nanoparticles, the PTTEMA2@BT based nanocomposite exhibits stored energy densities that are more than three times as large as the energy density stored in the PTTEMA homopolymer under the same applied field strength. Additionally, the inclusion of PPTEMA@BT nanoparticles has almost no negative effect on the energy

dx.doi.org/10.1021/cm502341n | Chem. Mater. 2014, 26, 5319−5326

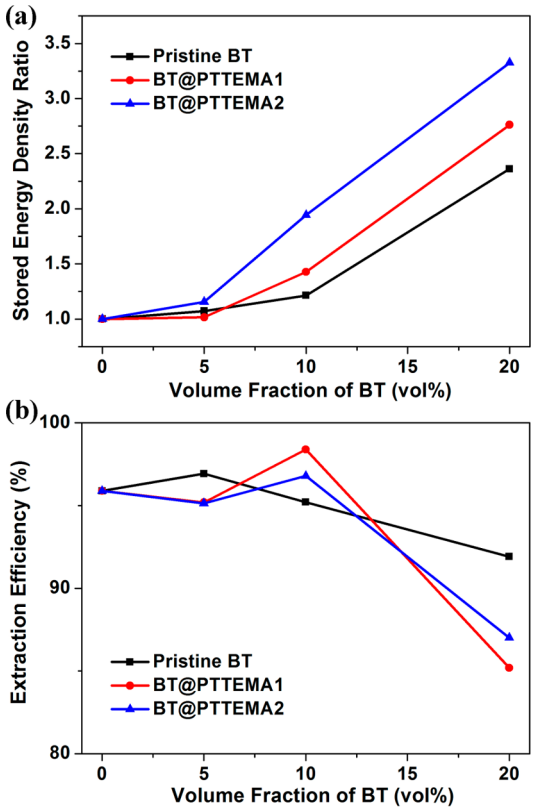

Figure 7. (a) Stored energy densities ratio and (b) Energy extraction efficiency of BT/PTTEMA and PTTEMA@BT/PTTEMA nanocomposites relative to a pure PTTEMA homopolymer measured at 210 kV cm^{-1} with 1 kHz cycle frequency, as a function of varying vol % loading of BT nanoparticles.

extraction efficiency at relatively low vol % loading of BT nanoparticles (≤10%, Figure 7b). With vol % loading up to 10%, the energy extraction efficiency is comparable to that of the pure PTTEMA homopolymer, which is higher than 95%. With the loading of BT nanoparticles further increased, a decrease in extraction efficiency was observed, probably due to the increased hysteresis (Figure 6a). However, the extraction efficiency is still higher than 85% at 20 vol % loading of BT nanoparticles. The percentage energy loss (Figure S12) is generally less than 10% for PTTEMA and BT/PTTEMA composites at low to moderate field strength.

III. CONCLUSION

In conclusion, a class of novel BT based polymer nanoparticles were prepared as nanodielectric materials. The oligothiophene-containing polymer was grafted from BT nanoparticles via surface-initiated RAFT polymerization in a controlled/"living" fashion. The robust surface control on chemistry and compositions manifests its impact on dielectric properties of these composites. Our results demonstrate that this novel nanocomposite system fulfilled the simultaneous achievement of both high permittivity and low dielectric loss over a wide range of frequency, indicating the great potential for application in nanodielectric energy storage. This surface engineering approach could be generalized to introduce other π-conjugated polarizable polymer shells to a variety of nanoparticles.

IV. EXPERIMENTAL SECTION

Materials. All reagents were purchased from Alfa Aesar and Sigma-Aldrich and used as received unless otherwise noted. 1,4-Dioxane was distilled over sodium and benzoquinone before use. 2-Mercaptothiazoline activation of 4-cyanopentanoic acid dithiobenzoate (CPDB) was carried out according to the methods in the literature.[52,53]

Characterization. ^{1}H NMR (300 MHz) spectra were recorded on a Varian Mercury 300 spectrometer with tetramethylsilane (TMS) as an internal reference. FT-IR spectra were recorded using a BioRad Excalibur FTS3000. Gel permeation chromatography (GPC) was performed at 50 °C on a Varian system equipped with a Varian 356-LC refractive index detector and a Prostar 210 pump. The columns were STYRAGEL HR1, HR2 (300 × 7.5 mm) from Waters. HPLC grade DMF with 0.01 wt % LiBr was used as eluent at a flow rate of 1.0 mL/min. Polystyrene standards were used for calibration. Mass spectrometry was conducted on a Waters Micromass Q-Tof mass spectrometer, and the ionization source was positive ion electrospray. Thermal transitions of the polymers were recorded by using differential scanning calorimetry (DSC) on a TA Instruments Q2000 in a temperature range from 0 to 200 °C at heating and cooling rates of 10 °C min^{-1} under constant nitrogen flow at a rate of 50 mL min^{-1}. Samples (between 3 and 5 mg) were added to aluminum hermetic pans and sealed. The data were collected during the second heating and cooling cycle. Thermogravimetric analysis (TGA) was conducted on a TA Instruments Q5000 using a heating rate of 10 °C min^{-1} from RT to 1000 °C under constant nitrogen flow. Wide-angle X-ray diffraction (WAXD) measurements were conducted on a Rigaku D/Max 2100 Powder X-ray Diffractometer (Cu Kα radiation) instrument. A Hitachi 8000 transmission electron microscope (TEM) operated with an accelerating voltage of 200 kV was used to acquire images of particles. TEM samples were prepared by dropping solution on carbon-supported copper grids and drying before observation. Tapping-mode atomic force microscopy (AFM) experiments were carried out using a Multimode Nanoscope V system (Veeco (now Bruker), Santa Barbara, CA). The measurements were performed using commercial Si cantilevers with a nominal spring constant and resonance frequency at 20−80 N/m and 230−410 kHz, respectively (TESP, Bruker AFM Probes, Santa Barbara, CA). The height and phase images were acquired simultaneously at the set-point ratio A/A_o = 0.9−0.95, where A and A_o refer to the "tapping" and "free" cantilever amplitudes, respectively. Field-Emission Scanning Electron Microscopy (FE-SEM, Zeiss UltraPlus, operated at 15 kV accelerating voltage) was used to acquire images of nanocomposite films.

Preparation of CPDB Anchored $BaTiO_3$ Nanoparticles. A tetrahydrofuran (THF) solution (25 mL) of the amino-functionalized $BaTiO_3$ nanoparticles (1.6 g) was sonicated for 30 min, and then a THF solution of activated CPDB (2.1 mL, 0.1 g mL^{-1}) was added dropwise into the suspension solution at 0 °C in ice bath. After complete addition, the solution was allowed to warm to room temperature and stirred overnight. The reaction mixture was then poured into a large amount of THF (100 mL). The particles were recovered by centrifugation at 8000 rpm for 10 min. The particles were then redissolved in 50 mL of THF and recentrifuged for several times until the supernatant layer after centrifugation was colorless. The CPDB anchored $BaTiO_3$ nanoparticles (BT-CPDB) were dried at room temperature (BT-CPDB: 1.5 g).

2-(2,2′:5′,2″-Terthien-5-yl)ethyl Methacrylate (TTEMA) Graft Polymerization from CPDB Anchored $BaTiO_3$ Nanoparticles (PTTEMA1@BT). CPDB anchored $BaTiO_3$ (0.80 g), free CPDB (5.78 mg, 0.02 mmol), TTEMA (2.98 g, 8.27 mol), azobis(isobutyronitrile) (AIBN) (3.05 mg, 0.02 mmol), and 6.56 mL of dry 1,4-dioxane were added to a 25 mL Schlenk flask and degassed by 5 cycles of freeze−pump−thaw. An initial sample was taken before the flask was submerged into a 90 °C preheated oil bath. Samples were taken out at predetermined intervals to monitor the reaction conversion by ^{1}H NMR before stopping the reaction. When conversion reached ca. 35−40%, the reaction flask was immediately cooled in ice bath, and the mixture was diluted with THF. The terthiophene-containing polymer modified $BaTiO_3$ particles were recovered by centrifugation at 8000

dx.doi.org/10.1021/cm502341n | Chem. Mater. 2014, 26, 5319−5326

rpm for 10 min. The PTTEMA@BT particles were then redissolved in 50 mL of THF and recentrifuged for several times until the supernatant layer after centrifugation was colorless. The free PTTEMA can also be recovered by combining all the clear supernatant-layer solutions after centrifugation, concentrated, purified by precipitation into cold hexane three times to remove any unreacted monomers, and vacuum-dried at room temperature (PTTEMA1@BT nanoparticles: 0.7 g).

General Procedures for Cleaving Graft Polymer from PTTEMA@BT Nanoparticles. In a typical experiment, 30 mg of PTTEMA@BT nanoparticles was dissolved in 2 mL of THF. Aqueous HF (49%, 0.1 mL) was added, and the solution was allowed to stir at room temperature overnight. The suspension solution was centrifuged, and the clear supernatant-layer solution in light yellow color was collected, concentrated, and precipitated in cold hexane. The recovered PTTEMA was then subjected to GPC analysis. Graft polymer from PTTEMA1@BT: M_n = 22,000 g mol^{-1} (GPC), $Đ$ = 1.12 (GPC) and that from PTTEMA2@BT: M_n = 32,400 g mol^{-1} (GPC), $Đ$ = 1.12 (GPC).

Dielectric Property Characterization. Composite films for dielectric property characterization were prepared by solution blending using THF. PTTEMA was dissolved in THF (35 mg mL^{-1}), and BT or PTTEMA@BT particles were suspended in THF with 1−2 h sonication. The solutions were blended, sonicated for an additional 30 min, and then poured in heavy-gauge aluminum pans. The THF was removed by evaporation at 44 °C under reduced pressure (635 mmHg absolute) for about 2 h without any post-treatment (thermal annealing). This resulted in films with uniform thickness and free of bubbles, cracks, or other defects. Film thicknesses were measured at multiple positions with a micrometer, in the range of 3−20 μm. Strips of aluminum pan bearing polymer or composite films were cut using scissors. The aluminum pan served as the bottom electrode for dielectric measurements. Gold was sputter-coated under argon atmosphere through a shadow mask to deposit circular gold electrodes (area 0.13 cm^2) on the films' top surfaces.

The complex impedance of polymer and composite film samples was measured using an impedance analyzer (Agilent model 4192A LF). Measurements were carried out at fixed applied voltage (10 mV) and varying frequency (typically 10^2 to 1.2 × 10^7 Hz). Impedance spectra were collected for 3−5 specimens of each sample to ensure reproducibility; average values are reported. The real and complex parts of the impedance, expressed as impedance magnitude and phase angle, were analyzed using a parallel RC circuit model describing a "leaky" capacitor, yielding values of relative permittivity (ε_{eff}) and loss tangent (tan δ) as functions of frequency.

Polarization measurements at higher applied voltages employed a Precision Multiferroic polarization tester (Radiant, Inc.). Polarization data (D versus E) were obtained for applied voltages up to 2000 V with a cycle frequency of 1.0 kHz. The maximum applied field strength depended on the sample film thickness and breakdown strength. Stored energy density ($\hat{W}_s$), was determined by numerical integration of E, according to $\hat{W} = \int E dD$, from D = 0 to the maximum value of D (D_{max}) achieved in the hysteresis loop. Recovered energy density ($\hat{W}_r$) was determined by numerically integrating E from D_{max} to the value of D where E = 0. Percentage energy extraction efficiency is computed as 100 × $\hat{W}_r/\hat{W}_s$.

■ ASSOCIATED CONTENT

Ⓢ Supporting Information

NMR, GPC, DSC, TGA, and relative permittivity, stored and recovered energy density, percentage energy loss of all the nanocomposites, D-E loops of PTTEMA1@BT/PTTEMA nanocomposites. This material is available free of charge via the Internet at http://pubs.acs.org.

■ AUTHOR INFORMATION

Corresponding Author

*E-mail: tang4@mailbox.sc.edu, ploehn@mailbox.sc.edu.

Notes

The authors declare no competing financial interest.

■ ACKNOWLEDGMENTS

This work was supported the Office of Naval Research (award N000141110191).

■ REFERENCES

(1) Jain, P.; Rymaszewski, E. J. *Thin Film Capacitors for Packaged Electronics*; National Academics: Washington, DC, 2003.
(2) Bhattacharya, S. K.; Tummala, R. R. *J. Mater. Sci.: Mater. Electron.* **2000**, *11*, 253.
(3) Barber, P.; Balasubramanian, S.; Anguchamy, Y.; Gong, S.; Wibowo, A.; Gao, H.; Ploehn, H. J.; zur Loye, H.-C. *Materials* **2009**, *2*, 1697−1733.
(4) Nalwa, H. S. *Handbook of Low and High Dielectric Constant Materials and Their Applications. Vol. 1: Materials and Processing. Vol. 2: Phenomena, Properties and Applications*; Academic Press: New York, 1999.
(5) Thongbai, P.; Yamwong, T.; Maensiri, S. *Appl. Phys. Lett.* **2009**, *94*, 152905.
(6) Zhu, J. L.; Jin, C. Q.; Cao, W. W.; Wang, X. H. *Appl. Phys. Lett.* **2008**, *92*, 242901.
(7) Haeni, J. H.; Irvin, P.; Chang, W.; Uecker, R.; Reiche, P.; Li, Y. L.; Choudhury, S.; Tian, W.; Hawley, M. E.; Craigo, B.; Tagantsev, A. K.; Pan, X. Q.; Streiffer, S. K.; Chen, L. Q.; Kirchoefer, S. W.; Levy, J.; Schlom, D. G. *Nature* **2004**, *430*, 758−761.
(8) Wilk, G. D.; Wallace, R. M.; Anthony, J. M. *J. Appl. Phys.* **2000**, *87*, 484−492.
(9) Lovinger, A. J. *Science* **1983**, *220*, 1115−1121.
(10) Zhang, Q. M.; Bharti, V.; Zhao, X. *Science* **1998**, *280*, 2101−2104.
(11) Chu, B. J.; Zhou, X.; Ren, K. L.; Neese, B.; Lin, M. R.; Wang, Q.; Bauer, F.; Zhang, Q. M. *Science* **2006**, *313*, 334−336.
(12) Lu, Y. Y.; Claude, J.; Neese, B.; Zhang, Q. M.; Wang, Q. *J. Am. Chem. Soc.* **2006**, *128*, 8120−8121.
(13) Zhu, L.; Wang, Q. *Macromolecules* **2012**, *45*, 2937−2954.
(14) Wu, S.; Li, W.; Lin, M.; Burlingame, Q.; Chen, Q.; Payzant, A.; Xiao, K.; Zhang, Q. M. *Adv. Mater.* **2013**, *25*, 1734−1738.
(15) Khanchaitit, P.; Han, K.; Gadinski, M. R.; Li, Q.; Wang, Q. *Nat. Commun.* **2013**, *4*, 2845.
(16) Wu, S.; Lin, M. R.; Lu, S. G.; Zhu, L.; Zhang, Q. M. *Appl. Phys. Lett.* **2011**, *99*, 132901.
(17) Chen, X. Z.; Li, Z. W.; Cheng, Z. X.; Zhang, J. Z.; Shen, Q. D.; Ge, H. X.; Li, H. T. *Macromol. Rapid Commun.* **2011**, *32*, 94−99.
(18) Xia, F.; Cheng, Z. Y.; Xu, H. S.; Li, H. F.; Zhang, Q. M.; Kavarnos, G. J.; Ting, R. Y.; Abdul-Sedat, G.; Belfield, K. D. *Adv. Mater.* **2002**, *14*, 1574−1577.
(19) Hardy, C. G.; Islam, M. S.; Gonzalez-Delozier, D.; Ploehn, H. J.; Tang, C. *Macromol. Rapid Commun.* **2012**, *33*, 791−797.
(20) Nguema, E.; Vigneras, V.; Miane, J. L.; Mounaix, P. *Eur. Polym. J.* **2008**, *44*, 124−129.
(21) Fattoum, A.; Arous, M.; Gmati, F.; Dhaoui, W.; Mohamed, A. B. *J. Phys. D: Appl. Phys.* **2007**, *40*, 4347−4354.
(22) Ho, J.; Ramprasad, R.; Boggs, S. *IEEE Trans. Dielectr. Electr. Insul.* **2007**, *14*, 1295−1301.
(23) Starkweather, H. W.; Avakian, P.; Matheson, R. R.; Fontanella, J. J.; Wintersgill, M. C. *Macromolecules* **1992**, *25*, 6871−6875.
(24) Hardy, C. G.; Islam, M. S.; Gonzalez-Delozier, D.; Morgan, J. E.; Cash, B.; Benicewicz, B. C.; Ploehn, H. J.; Tang, C. *Chem. Mater.* **2013**, *25*, 799−807.
(25) Wang, Q.; Zhu, L. *J. Polym. Sci., Part B: Polym. Phys.* **2011**, *49*, 1421−1429.
(26) Dang, Z. M.; Yuan, J. K.; Zha, J. W.; Zhou, T.; Li, S. T.; Hu, G. H. *Prog. Mater. Sci.* **2012**, *57*, 660−723.
(27) Nelson, J. K. *Dielectric Polymer Nanocomposites*; Springer: New York, 2010.

(28) Li, Z.; Fredin, L. A.; Tewari, P.; DiBenedetto, S. A.; Lanagan, M. T.; Ratner, M. A.; Marks, T. J. *Chem. Mater.* **2010**, *22*, 5154−5164.
(29) Dang, Z. M.; Zhou, T.; Yao, S. H.; Yuan, J. K.; Zha, J. W.; Song, H. T.; Li, J. Y.; Chen, Q.; Yang, W. T.; Bai, J. *Adv. Mater.* **2009**, *21*, 2077−2082.
(30) Paniagua, S. A.; Kim, Y.; Henry, K.; Kumar, R.; Perry, J. W.; Marder, S. R. *ACS Appl. Mater. Interfaces* **2014**, *6*, 3477−3482.
(31) Yang, K.; Huang, X.; Xie, L.; Wu, C.; Jiang, P.; Tanaka, T. *Macromol. Rapid Commun.* **2012**, *33*, 1921−1926.
(32) Xia, F.; Cheng, Z. Y.; Xu, H. S.; Li, H. F.; Zhang, Q. M.; Kavarnos, G. J.; Ting, R. Y.; Abdul-Sedat, G.; Belfield, K. D. *Adv. Mater.* **2002**, *14*, 1574−1577.
(33) Kofod, G.; Risse, S.; Stoyanov, H.; McCarthy, D. N.; Sokolov, S.; Kraehnert, R. *ACS Nano* **2011**, *5*, 2412−2413.
(34) Guo, N.; DiBenedetto, S. A.; Tewari, P.; Lanagan, M. T.; Ratner, M. A.; Marks, T. J. *Chem. Mater.* **2010**, *22*, 1567−1578.
(35) Luo, X.; Zhao, X.; Xu, S.; Wang, B. *Polymer* **2009**, *50*, 796−801.
(36) Clayton, L. M.; Sikder, A. K.; Kumar, A.; Cinke, M.; Meyyappan, M.; Gerasimov, T. G.; Harmon, J. P. *Adv. Funct. Mater.* **2005**, *15*, 101−106.
(37) Bobnar, V.; Levstik, A.; Huang, C.; Zhang, Q. M. *Phys. Rev. Lett.* **2004**, *92*, 047604.
(38) Dang, Z. M.; Lin, Y. H.; Nan, C. W. *Adv. Mater.* **2003**, *15*, 1625−1629.
(39) Li, J. J.; Seok, S. I.; Chu, B. J.; Dogan, F.; Zhang, Q. M.; Wang, Q. *Adv. Mater.* **2009**, *21*, 217−221.
(40) Li, J. J.; Khanchaitit, P.; Han, K.; Wang, Q. *Chem. Mater.* **2010**, *22*, 5350−5357.
(41) Yang, K.; Huang, X.; Huang, Y.; Xie, L.; Jiang, P. *Chem. Mater.* **2013**, *25*, 2327−2338.
(42) Kim, P.; Jones, S. C.; Hotchkiss, P. J.; Haddock, J. N.; Kippelen, B.; Marder, S. R.; Perry, J. W. *Adv. Mater.* **2007**, *19*, 1001−1005.
(43) Kim, P.; Doss, N. M.; Tillotson, J. P.; Hotchkiss, P. J.; Pan, M.-J.; Marder, S. R.; Li, J.; Calame, J. P.; Perry, J. W. *ACS Nano* **2009**, *3*, 2581−2592.
(44) Tan, S. B.; Hu, X.; Ding, S. J.; Zhang, Z. C.; Li, H. Y.; Yang, L. J. *J. Mater. Chem. A* **2013**, *1*, 10353−10361.
(45) Wen, F.; Xu, Z.; Tan, S. B.; Xia, W. M.; Wei, X. Y.; Zhang, Z. C. *ACS Appl. Mater. Interfaces* **2013**, *5*, 9411−9420.
(46) Roy, M.; Nelson, J. K.; McCrone, R. K.; Schadler, L. S.; Reed, C. W.; Keefe, R.; Zeneger, W. *IEEE Trans. Dielectr. Electr. Insul.* **2005**, *12*, 629−643.
(47) Calebrese, C.; Hui, L.; Schadler, L. S.; Nelson, J. K. *IEEE Trans. Dielectr. Electr. Insul.* **2011**, *18*, 938−945.
(48) Schadler, L. S.; Brinson, L. C.; Sawyer, W. G. *J. Mater.* **2007**, *25*, 53−61.
(49) Yang, K.; Huang, X. Y.; Zhu, M.; Xie, L. Y.; Tanaka, T.; Jiang, P. K. *ACS Appl. Mater. Interfaces* **2014**, *6*, 1812−1822.
(50) Xie, L. Y.; Huang, X. Y.; Huang, Y. H.; Yang, K.; Jiang, P. K. *J. Phys. Chem. C* **2013**, *117*, 22525−22537.
(51) Qiao, Y. L.; Islam, M. S.; Han, K.; Leonhardt, E.; Zhang, J. Y.; Wang, Q.; Ploehn, H. J.; Tang, C. B. *Adv. Funct. Mater.* **2013**, *23*, 5638−5646.
(52) Xie, L.; Huang, X.; Wu, C.; Jiang, P. *J. Mater. Chem.* **2011**, *21*, 5897−5906.
(53) Li, C.; Han, J.; Ryu, C. Y.; Benicewicz, B. C. *Macromolecules* **2006**, *39*, 3175−3183.
(54) Wang, L.; Benicewicz, B. C. *ACS Macro Lett.* **2013**, *2*, 173−176.
(55) Zhu, X. H.; Zhu, J. M.; Zhou, S. H.; Liu, Z. G.; Ming, N. B.; Hesse, D. *Solid State Phenom.* **2005**, *106*, 41−46.
(56) Zhu, L.; Calhoun, B. H.; Ge, Q.; Quirk, R. P.; Cheng, S. Z. D.; Thomas, E. L.; Hsiao, B. S.; Yeh, F.; Liu, L. Z.; Lotz, B. *Macromolecules* **2001**, *34*, 1244−1251.
(57) Guo, N.; DiBenedetto, S. A.; Kwon, D.-K.; Wang, L.; Russell, M. T.; Lanagan, M. T.; Facchetti, A.; Marks, T. J. *J. Am. Chem. Soc.* **2007**, *129*, 766−767.
(58) Fredin, L. A.; Li, Z.; Ratner, M. A.; Lanagan, M. T.; Marks, T. J. *Adv. Mater.* **2012**, *24*, 5946−5953.